Fizika Nizkikh Temperatur, 2000, v. 26, Nos. 9/10, p. 963–971

# FTIR studies of annealing processes and irradiation effects at 266 nm in ozone-amorphous ice-mixtures

H. Chaabouni, L. Schriver-Mazzuoli, and A. Schriver

*Laboratoire de Physique Moléculaire et Applications**, *Unité propre du CNRS, Université Pierre et Marie Curie, Tour 13, case 76, 4 place Jussieu 75252 Paris Cedex 05, France*
E-mail: schriver@ccr.jussieu.fr

Received March 14, 2000

Fourier Transform Infrared (FTIR) Spectroscopy is used to study the vibrational spectroscopy of ozone trapped in amorphous ice (a situation observed on icy satellites in the solar system). Evaporation of ozone from ice is investigated from 30 to 150 K under a static pressure of $10^{-7}$ Torr. Condensed and chemisorbed ozone on the surface of micropores is released at a temperature between 40 and 80 K, and ozone in water lattice evaporates starting from 120 K. The release of ozone probes the gradual transformation of water ice. The photochemistry of ozone in excess ice is also investigated using 266 nm laser irradiation. At low temperature, condensation of mixtures $H_2O/O_3$ leads to ozone trapped in pores and cavities, and $H_2O_2$ is produced through the hydrogen bonded complex between ozone and free OH bonds. At higher temperature, when a solid solution of ozone in water is observed, $H_2O_2$ is formed by the reaction of the excited oxygen atom O ($^1D$) with the nearest water molecules. Kinetic studies suggest that recombination of the dioxygen molecule with ground-state atomic oxygen O ($^3P$) is a minor channel.

PACS: 78.30.Hv, 71.55.Ht

## 1. Introduction

Due to the importance of ozone in the atmosphere, infrared spectra of isotopic and natural ozone have been widely studied in the gas phase and in various matrices [1]. Recently, from observations by the Hubble Space Telescope, oxygen and ozone have been recently identified on Ganymede (a satellite of Jupiter) [2–5] and on Rhea and Dione (two Saturnian satellites) [6]. All these satellites have surfaces rich in water ice. Oxygen, which resides in a condensed state at the surface of Ganymede in spite of the temperature range (80 to 140 K, depending on the latitude), is produced from decomposition of water molecules in the surface ice by plasma bombardment. Thanks to defect-trapping bubble production by the ion fluxes [7], surface adsorption, and clathrate formation, a large fraction of oxygen can stay in small ice voids. Dissociation of oxygen by UV photons or incident ions produces ozone, which in turn dissociates. Competition between active production and destruction of ozone leads to an $O_2$–$O_3$ equilibrium. On Ganymede the density ratio of $[O_3]/[O_2]$ was estimated to be $10^{-4}$ to $10^{-3}$ [4], a value in agreement with Chapmann equations [8] including quenching of O ($^1D$) by $O_2$ and $O_3$ . Although there is a general understanding of the processes involved, a quantitative understanding has not be achieved. In the present work we describe the IR spectra of ozone–water mixtures at low temperature, and then we examine the capacity of amorphous water ice for trapping $O_3$ at temperatures between 15 and 150 K. Finally, photodissociation of ozone in ice at 266 nm is reported. Ten years ago, as a part of their studies on photochemistry of solid ozone, Sedlacek and Wight mentioned briefly that irradiation of ozone in excess ice produced hydrogen peroxide, HOOH [9]. We confirm this observation and show that there are two origins for $H_2O_2$ formation: first a low-temperature one due to an ozone monolayer chemisorbed at the surface of the pores, and another one at higher temperature due to ozone which has diffused in the water ice lattice.

* Laboratoire Associé à l'Université P. et M. Curie

## 2. Experimental

The helium gas used was supplied by Air Liquide (N55). Water vapor was taken from distilled water (Prolabo for chromatography) which was first subjected to several degassing cycles under vacuum. Ozone was prepared from oxygen (Air Liquide N50) contained in a glass vacuum finger excited by a Tesla-coil discharge with trapping of ozone at liquid nitrogen temperature. Residual oxygen was removed by a freeze–pump–thaw cycle with liquid nitrogen. Water–ozone gas mixtures were deposited onto a gold-plated mirror with helium as carrier gas. Above 15 K, helium does not condense. Several $H_2O/O_3/He$ mixtures with different ratios of $O_3$ and $H_2O$ were prepared. The total pressures of ozone and water were typically 12 Torr, and the pressure of helium was 150 Torr. Cooling was provided by an Air Product Displex 202A rotating closed-cycle refrigerator with KBr optical windows for performing IR measurements and one quartz window for UV photolysis. The static pressure was $10^{-7}$ Torr. The temperature of the metal substrate was controlled by a silicon diode (Scientific Instruments 9600-1). The gas mixture was deposited via a capillary with a rate of 6 mmol·h$^{-1}$. The deposition nozzle parameters were 1 mm inner diameter and a distance of 20 mm from the gold substrate. The thickness of the layers was typically less than 500 nm. The spectra were recorded with a FTIR Bruker IFS 113 v spectrometer in the reflection mode (angle of incidence 5° from the normal to the surface). The nominal resolution was 0.5 and 2 cm$^{-1}$. Ozone photodissociation was carried out at 266 nm using the fourth harmonic of a Nd–YAG laser (YG 781C-20 from Quantel) which operates at 20 Hz with a 4-ns pulse duration. The initial power was adjusted to 10–25 mJ per pulse. The light intensity was spatially homogenized with a divergent lens placed in front of the cryostat UV window. The fluence inside the cryostat was estimated from the power measured with a PSV 3102 Gentic S/N 61592 detector with a cross section of 1.76 cm$^2$ that was placed after the lens and a $CaF_2$ window simulating the entrance window of the cryostat.

## 3. Spectroscopy

### 3.1. Water ice

At low pressure and temperature, water ice exists in metastable states which are not in thermodynamic equilibrium. All structural transitions are time-dependent and irreversible [10]. Water vapor deposition below 30 K results in the formation of high-density amorphous ice (1.1 g·cm$^{-3}$), generally labeled as $I_{ah}$, which has a great degree of polymorphism depending primarily upon the deposition conditions. Between 30 and 70 K, $I_{ah}$ transforms gradually into another, more ordered amorphous ice, labeled low-density ice, $I_{al}$ (0.94 g·cm$^{-3}$) which exists till about 130 K. At the glass transition temperature 127–133 K, $I_{al}$ transforms into a third amorphous phase, called the «restrained phase» ($I_{ar}$), which has the character of a strong liquid and which coexists with cubic ice $I_c$ from 130 to 220 K. The transition of both $I_c$ and $I_{ar}$ in hexagonal ice is only observed under confinement pressure at 195–223 K. Crystalline ice is converted to amorphous ice by ion irradiation [11,12] and short-wavelength UV irradiation [13].

Amorphous ice is microporous, with a wide pore size distribution (from 10 to 30 Å). Apparent surface areas have been calculated from gas adsorption isotherms. According to deposition temperature and hence to the morphology of the amorphous ice, the surface areas can vary from about 40 to about 200 m$^2$·g$^{-1}$ [14–16]. Thus the density which is measured from the compact bulk depends on the number and the distribution of voids and can reach values of less than 0.75 cm$^{-3}$ [17].

Numerous studies have been devoted to the IR spectra of ice because the coupled $\nu_{OH}$ band, the band most studied up to now, reflects the structure of ice, and its shape and the frequency of its maximum can therefore be used to distinguish the different forms of ice between 10 and 160 K. A thorough description of the absorptions of water under our experimental conditions has been recently reported [18]. Spectral effects on the $\nu_{OH}$ stretching band related to structural differences are discussed in light of previous works. Figure 1 compares typical spectra of ice films deposited at different temperatures. High-density amorphous ice ($I_{ah}$) ($T < 30$ K) has a strong polymorphism, and according to the deposition rates the broad band around 3380 cm$^{-1}$ is often accompanied by secondary maxima as illustrated in Fig. 1 (traces *a*, *b*, *c*). Narrow bands observed at about 3690 and 3671 cm$^{-1}$ are assigned to free OH bonds (dangling bands) of water clusters. The more ordered low-density amorphous phase ($I_{al}$) is characterized by a band at about 3250 cm$^{-1}$ (whatever the deposition type) with a shoulder at 3380 cm$^{-1}$, corresponding to a small amount of high-density amorphous ice which persists over extended periods of time and above 130 K. In our configuration, no dangling OH band at 3699 cm$^{-1}$, characterizing triple coordinated water molecules at the surface, were observed, perhaps because of orientation effects or to their weak-

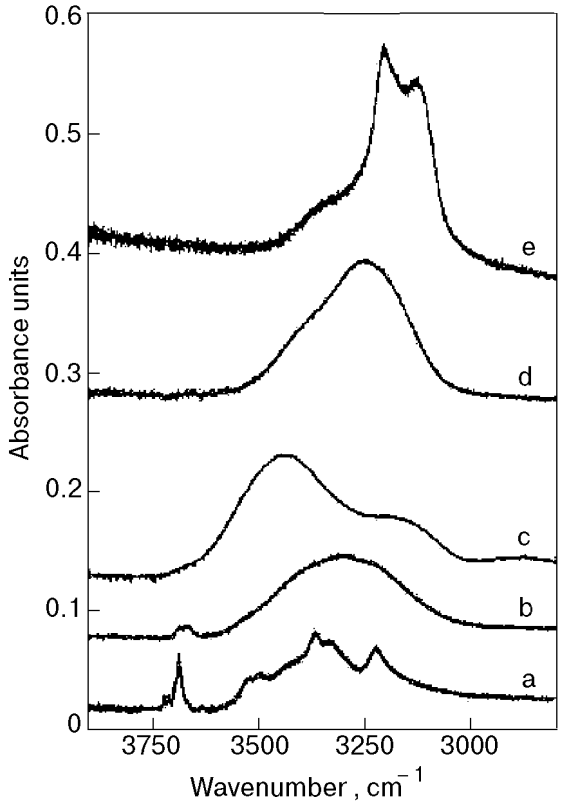


*Fig. 1.* Typical infrared spectra in the $\nu_{OH}$ region of water ice films deposited: at 11 K with different deposition rates, μmol·h$^{-1}$: 0.06 (*a*), 2 (*b*), 6 (*c*); at 70 K (*d*); at 150 K (*e*).

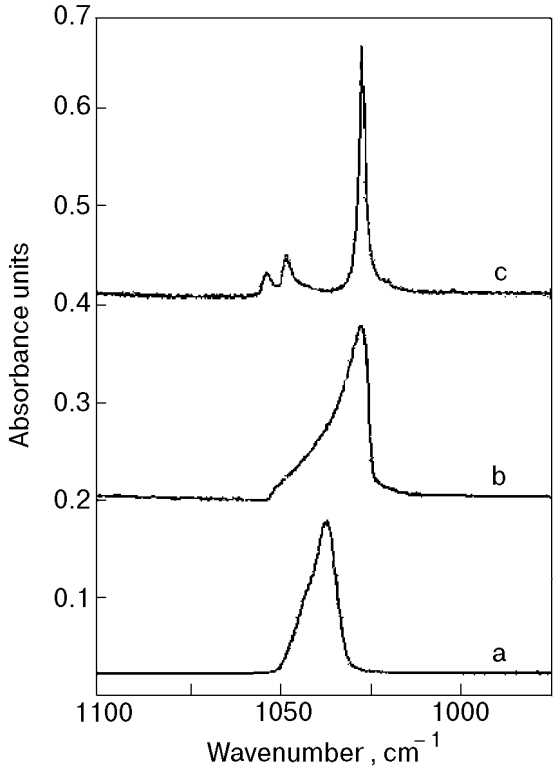


*Fig. 2.* FTIR spectra in the $\nu_3$ region of condensed films of ozone deposited on Au substrates at different temperatures *T*, K: 11 (*a*); 30 (*b*); 55 (*c*).

ness. When $I_{al}$ is obtained by annealing of a $I_{ah}$ film we observe an increase in intensity of the broad coupled $\nu_{OH}$ band due to formation of OH...O bonds. Spectra of water ice deposited directly at 150–160 K or obtained by annealing of amorphous ice above 130 K are characterized by a partially resolved doublet at about 3200 and 3130 cm$^{-1}$.

### 3.2. Solid ozone

As previously reported [19], solid ozone has two solid phases, an amorphous phase which is obtained below 11 K and a crystalline phase which is obtained above 50 K. Over the temperature range 11–50 K, condensation of ozone results in a mixture of disordered and ordered phases. The amorphous phase is stable until 50 K and the crystalline phase sublimes from 61 K with an activation energy of (23 ± 2) kJ·mol$^{-1}$.

Representative spectra of ozone deposited at different temperatures are shown in Fig. 2 in the $\nu_3$ region of ozone. As can be seen, the $\nu_3$ band, the most intense in the gas phase or in matrices, shifts from 1037.0 cm$^{-1}$ to 1026.2 cm$^{-1}$ and narrows, with a full width at half maximum (FWHM) from 9.1 cm$^{-1}$ to 1.4 cm$^{-1}$, when going from the amorphous to the crystalline phase. The two satellites features measured at 1054.4 and 1048.0 cm$^{-1}$ in the spectrum of crystalline ozone have been tentatively assigned to clusters of ozone formed in the gas phase. Characteristics of other bands (fundamentals and combinations) are given in Ref. 19.

### 3.3. Water/ozone mixtures

In order to examine the effect of water ice on the spectrum of ozone, several mixtures with different $H_2O/O_3$ ratios (from 0.25 to 10) were deposited at 30 K with helium as the carrier gas. Higher ratios could not be accurately studied due to the weakness of ozone in thin ice films. Figure 3 compares the spectra of some films with different compositions. In the $\nu_3$ region of ozone, the spectrum of the sample rich in ozone (trace *a*) is nearly similar to the spectrum of pure ozone deposited at 30 K (see Fig. 2, trace *b*). With water concentration increase, the $\nu_3$ ozone band broadens, becomes more symmetrical, and shifts weakly towards high frequency. However, small changes were observed in the profile of the band from one sample to another with similar composition, indicating that ozone in ice is in different states depending on the condensation process, as discussed below. In the less ozone-rich film (trace *d*

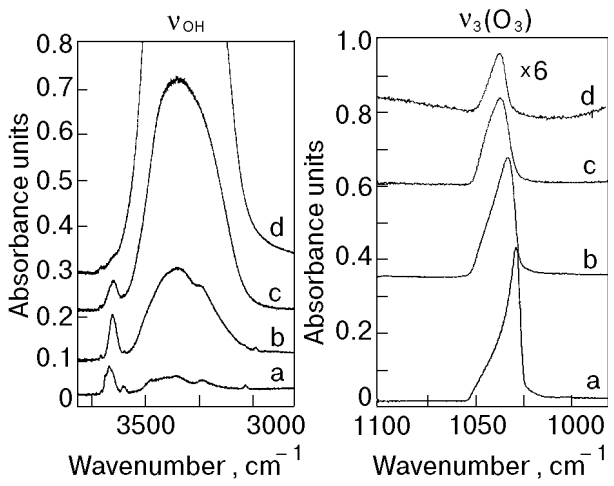


*Fig. 3.* Infrared spectra in water $\nu_{OH}$ and ozone $\nu_3$ regions of $H_2O/O_3$ mixtures deposited at 30 K. Initial ratio: 0.25 (*a*); 1 (*b*); 5 (*c*); 10 (*d*).

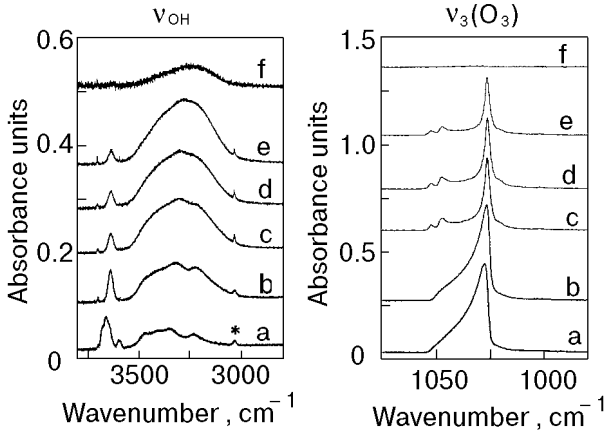


*Fig. 4.* Annealing effects on the $\nu_{OH}$ band of water and on the $\nu_3$ band of ozone after deposition at 30 K of a $H_2O/O_3$ mixture rich in ozone ($H_2O/O_3$ = 0.25): after deposition at 30 K (*a*); after successive annealing at different temperatures *T*, K: 50 (*b*); 55 (*c*); 60 (*d*); 65 (*e*); 70 (*f*). All spectra are recorded at the annealing temperature. (* is $3\nu_3$ band of ozone).

of Fig. 3) the $\nu_3$ absorption appeared as a nearly symmetrical band with a maximum at 1035.6 $cm^{-1}$ and a FWHM of 10.2 $cm^{-1}$. In the $\nu_{OH}$ region of water, a new band located between 3647 $cm^{-1}$ and 3640 $cm^{-1}$, depending on the composition, appeared due to the interaction of ozone with water molecules having a free OH bond. Such a band (hereafter labeled $D_{ga}$) was also observed when ozone was deposited on the surface of a thin water film, and it was assigned to a monolayer of ozone hydrogen bonded to water molecules in the bulk pores of amorphous ice [19]. In the mixture rich in ozone this band appeared as a shoulder on the dangling bands at 3683 and 3666 $cm^{-1}$ characterizing free OH groups of water clusters.

In spite of premixing of the water and ozone gases, experiments showed that condensation of ozone/water mixtures at low temperature has different efficiency and leads to several uncontrolled metastable states of ozone. As a matter of fact, the ratio between integrated intensities of the $\nu_{OH}$ coupled band and of the $\nu_3$ ozone band was not accurately correlated to the initial ratio of $H_2O/O_3$ pressures. In the same manner, the ratio between integrated intensities of the perturbed OH band at 3640.5 $cm^{-1}$ ($D_{ga}$) and of the $\nu_3$ ozone band varied from 0.7 to 3 for films having the same initial composition. Amorphous ice is a disordered material containing pores, cracks, voids, and capillarities, into which ozone can penetrate. According to the composition, codeposition of $H_2O/O_3$ samples on cold substrates at 30 K can generate separate ozone layers on the amorphous ice surface, ozone large clusters trapped in the ice, a monolayer of ozone molecules hydrogen-bonded to water in the pores, condensed ozone in the pores or cracks, and, probably, only a very small amount of ozone in substitutional sites of the ice lattice.

## 4. Temperature effects

Two sets of experiments were carried out. In the first set, after deposition at 30 K the mixed films were annealed at 160 K at a rate of 5 K·$min^{-1}$, and successive spectra were recorded after each temperature increase. In the second set, mixed films were deposited directly at 70 K.

### *4.1. Mixtures deposited at 30 K*

*4.1.1. Mixtures rich in ozone.* Figure 4 shows the evolution with temperature of a spectrum of a initial mixture rich in ozone ($H_2O/O_3$ = 0.25). Between 30 and 50 K, the intensity of the $\nu_3$ band of ozone and of the associated dangling band $D_{ga}$ at 3647.5 $cm^{-1}$ remained unchanged, while the $\nu_{OH}$ band of water increased in intensity, indicating that $I_{ah}$ begins to transform into $I_{al}$, with the loss of the 3683 and 3666 $cm^{-1}$ features assigned at free OH in clusters. Only the frequency of the $D_{ga}$ absorption shifted from 3647.5 $cm^{-1}$ to 3642.4 $cm^{-1}$. In the 50–55 K temperature range, amorphous ozone (multilayers and ozone in interaction with water) disappeared, as monitored by the disappearance of the high frequency of the $\nu_3$ band and the decrease in intensity of the $D_{ga}$ feature, which was now located at 3640.5 $cm^{-1}$. From 55 to 60 K the spectra remained unchanged. Above 60 K, crystalline ozone (multilayers and ozone in interaction with water)

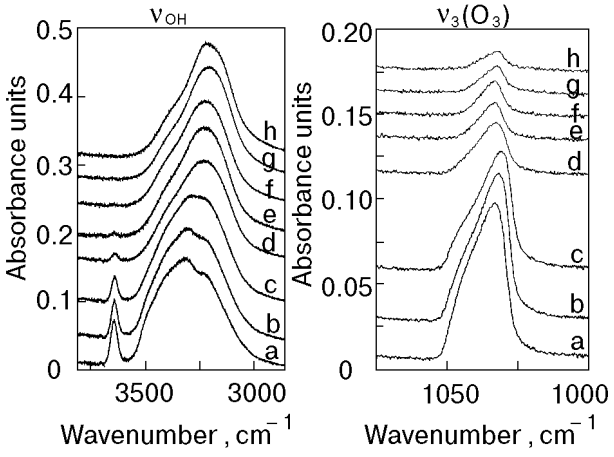


*Fig. 5.* Spectral changes with temperature in the $\nu_{OH}$ region of water and in the $\nu_3$ region of ozone after deposition at 30 K of a $H_2O/O_3$ mixture rich in water ($H_2O/O_3 = 3$): after deposition at 30 K (*a*); after annealing at different temperatures *T*, K: 50 (*b*); 60 (*c*); 70 (*d*); 80 (*e*); 120 (*f*); 140 (*g*); 150 (*h*).

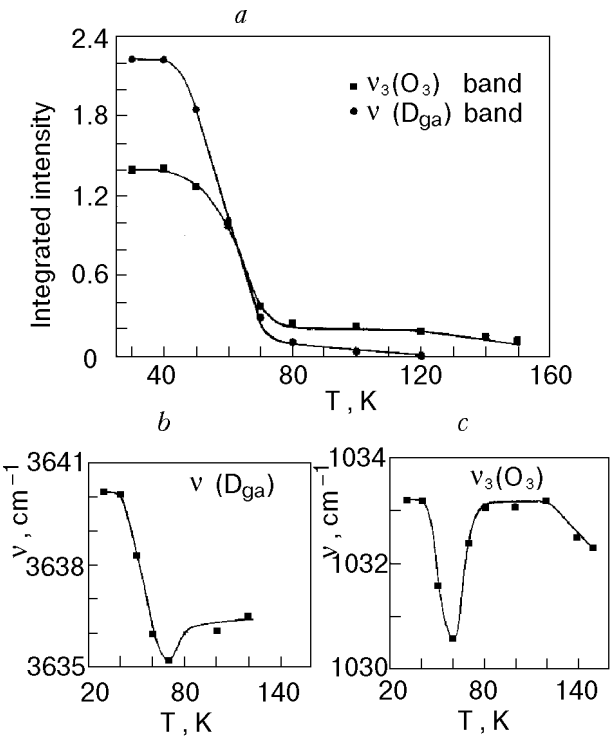


*Fig. 6.* Integrated band intensities as a function of temperature for the associated ozone dangling band and ozone $\nu_3$ band of the experiment presented in Fig. 5 (*a*). Temperature dependence of frequencies of the associated OH band (3640 $cm^{-1}$) (*b*) and the $\nu_3$ ozone band (1033 $cm^{-1}$) (*c*) of the experiment presented in Fig. 5.

began to evaporate and disappeared totally at 70 K. Water ice also disappeared nearly totally at 70 K along with the ozone.

The overall behavior of water between 30–60 K, similar to that of a pure water film, suggests that water molecules trapped in the ozone matrix probably diffuse in the ozone as the temperature increases, forming islands of water molecules which stay inside the ozone and sublimate when the ozone desorbs.

*4.1.2. Mixtures rich in water.* As expected, a great difference was found between films rich in ozone, which sublimate at 70 K, and films rich in water, which evolve nearly in the same manner for initial ratios $H_2O/O_3$ ranging from 2 to 10. Figure 5 shows typical spectra of an $H_2O/O_3$ film (initial ratio 3) deposited at 30 K and gradually annealed at 150 K, and Fig. 6 presents the evolution of the integrated intensities of the $\nu_3$ ozone band and of the $D_{ga}$ band as a function of temperature as well as the evolution of the frequencies of the $\nu_3$ ozone band and the associated OH band ($D_{ga}$) with temperature. Two distinct ranges of ozone release are observed. The first part starts at 50 K and stops at 80 K. The second part starts at 120 K and is totally exhausted when the sample is kept at 150 K. The same trend was observed in other experiments, except that in some, but not all,of the more water-rich samples ozone remained at 160 K, suggesting that the formation of a local hydrate clathrate could occur by rearrangement in the solid state, depending on the mixture composition as well as condensation and annealing processes. Indeed, ozone release, which is in competition with ozone diffusion in the bulk of water at temperatures higher than 60 K [19], results from changes in the ice morphology. Between 50 to 80 K the release of ozone condensed in the pores parallels the structural transformation of amorphous high-density ice into low-density amorphous ice, as monitored by the evolution of the $\nu_{OH}$ band shape. Between 50 to 60 K few changes are observed, and the intensity of the $\nu_3$ ozone band weakly diminishes. Between 60 to 70 K the transformation is achieved, and a strong decrease of the $\nu_3$ ozone band is observed. Upon warming, the pores collapse and the part of the ozone trapped in the pores is released. From 120 to 150 K low-density amorphous ice transforms into crystalline ice, and the rearrangement of water molecules opens some of the blocked channels and results in the loss of diffused ozone in substitutional water sites. These results are similar to previous findings for the release of $CH_4$ , Ar, $N_2$ , Ne, $H_2$ [20,21] and CO [21–24] from water ice.

As is seen from Fig. 6, the profile and the frequency of the $\nu_3$ ozone absorption change with the temperature. In the 30–60 K temperature range,

the initial band at 1033.2 $cm^{-1}$ (FWHM = 17 $cm^{-1}$) shifts gradually at 1030.6 $cm^{-1}$. Above 80 K, a narrower, nearly symmetric band (FWHM = = 10.2 $cm^{-1}$) clearly emerges and shifts from 1033.1 to 1032.3 $cm^{-1}$ between 120 and 150 K. In fact, the $\nu_3$ ozone band is a composite of several overlapping bands which probe the annealing-produced changes in the surrounding water solid and the diffusion of ozone in water ice. The OH dangling bond in interaction with ozone is also very sensitive to the structural change of ice with temperature, but warming of the ice substrate affects this band differently than that of the $\nu_3$ ozone band. From 40 to 80 K, it diminishes monotonically and shifts from 3640.1 to 3636.1 $cm^{-1}$. This band probes, the collapse of the pores, which begins at 40 K without the release of ozone at this temperature; ozone begins to sublimate from 50 K. Traces of this band are observed between 80 to 120 K but not above 120 K, indicating that the crystalline ice is nonporous.

### *4.2. Mixtures rich in water deposited at 70 K*

Direct deposition of mixtures above 80 K showed that ozone was not trapped in water ice. Deposition at 70 K, a temperature at which solid ozone sublimes, led to a solid solution of ozone in water. Ozone appeared as a very weak band at a frequency in agreement with that observed previously between 80–120 K and with a comparable intensity for the same initial composition. When the temperature was increased from 140 to 160 K, ozone was slowly released, but a part remained in the bulk until evaporation of the water. This behavior might be an indication of the formation of local clathrates, as suggested previously, but it could also be due to ozone locked in deep voids without the possibility of release.

Overall, the experiments described above show that ozone that is produced on icy satellites of the solar system by photodissociation of oxygen can be kept inside water ice at temperatures higher than 120 K.

## 5. Irradiation effects

Irradiation with the 266 nm laser line (photon flux = $5 \cdot 10^{16}$ photons$\cdot cm^{-2} \cdot s^{-1}$) was carried out at 17 K, first on $H_2O/O_3$ mixtures rich in water deposited at 17 K and then on a mixture annealed at 130 K and cooled at 17 K. In mixtures deposited at 17 K, ozone is mainly trapped in pores and voids as probed by the strong $D_{ga}$ band at 3636 $cm^{-1}$, while in the preannealed mixture ozone resides mainly in the water lattice.

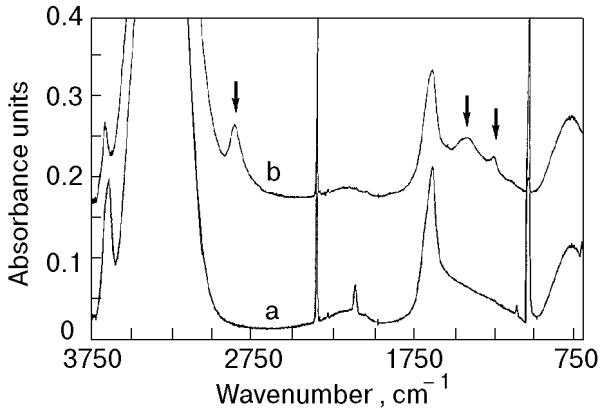


*Fig. 7.* 3750–700 $cm^{-1}$ region in the spectrum of a $H_2O/O_3$ mixture ($H_2O/O_3$ = 4): after deposition at 17 K (*a*); after irradiation at 17 K for 80 min with a 266 nm laser line (photon flux = $5 \cdot 10^{16}$ photons$\cdot cm^{-2} \cdot s^{-1}$) (*b*). New bands which appear after irradiation are indicated by arrows .

At an incident wavelength of 266 nm ozone produces atoms $O(^1D)$ and $O(^3P)$ with primary quantum yields of 0.83 and 0.17, respectively [25].

### *5.1. Mixtures deposited at 17 K*

Figure 7 compares in the 3750–700 $cm^{-1}$ region a typical spectrum recorded after deposition at 17 K with a spectrum recorded at 17 K after 80 min of irradiation corresponding to the total disappearance of ozone. After irradiation, two weak, broad bands at 2858 $cm^{-1}$ and 1425 $cm^{-1}$ (FWHM = 79 $cm^{-1}$and 102 $cm^{-1}$, respectively), with a weak feature at 1256 $cm^{-1}$ appeared. These two new bands can be unambiguously assigned to hydrogen peroxide according to published data [26]. They are quite comparable in frequency and width to bands observed in the spectrum of amorphous hydrogen peroxide deposited at 83 K, as shown in Fig. 1 of Ref. 26. They correspond to the ($2\nu_2$ , $\nu_2 + \nu_6$ , $2\nu_6$) and $\nu_2$ modes of $H_2O_2$ , respectively. The weak band at 1256 $cm^{-1}$ can be assigned to the $\nu_6$ mode.

Figure 8 shows the key regions of spectra recorded after different irradiation times. After 100 seconds, the $D_{ga}$ band disappears totally, the 2858 $cm^{-1}$ absorption of $H_2O_2$ nearly reaches its maximum in intensity and the $\nu_3$ ozone band is reduced to 17% of its initial intensity. Upon subsequent photolysis the ozone that remains in the lattice disappears totally after 80 min of irradiation, with only a weak increase in intensity of the 2858 $cm^{-1}$ absorption. These results are an indication that in this experiment the formation of hydrogen peroxide is mainly due to photodissociation of ozone chemisorbed on the water surface of micropores. In the $-O-H : O_3$ complex, $H_2O_2$ is formed

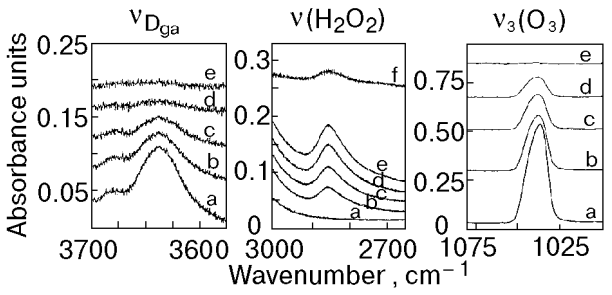


*Fig. 8.* Comparison of the spectra in the 3700–3575 $cm^{-1}$, 3000-2650 $cm^{-1}$ and 1080–1000 $cm^{-1}$ regions of a $H_2O/O_3$ mixture ($H_2O/O_3$ = 4): after deposition at 17 K (*a*); after irradiation at 17 K with a 266 nm laser line (photon flux = $5{\cdot}10^{16}$ photons·$cm^{-2}$·$s^{-1}$) for 20 s (*b*), 40 s (*c*), 100 s (*d*), 80 min (*e*). Difference spectrum between (*e*) and (*d*) is (*f*).

by the transfer of an oxygen atom from ozone to $H_2O$. Such behavior is in agreement with previous studies in matrices. In an argon matrix, irradiation of the isolated one-to-one complex $H_2O : O_3$ also led to the formation of $H_2O_2$ [27].

Kinetic studies of the disappearance of ozone and appearance of $H_2O_2$ were carried out. The decrease in the concentration of ozone was tracked by the decrease of the integrated intensity $A$ of the $D_{ga}$ absorption at 3636 $cm^{-1}$ and of the $\nu_3$ ozone absorption. The increase of the concentration of hydrogen peroxide was monitored by the increase of the integrated intensity $A$ of the 2858 $cm^{-1}$ absorption peak, which reached an asymptotic limit $A^{\infty}$ at long times. Plots of $\ln (A^0_{O_3}/A^t_{O_3})$, $\ln (A^0_{D_{ga}}/A^t_{D_{ga}})$, and

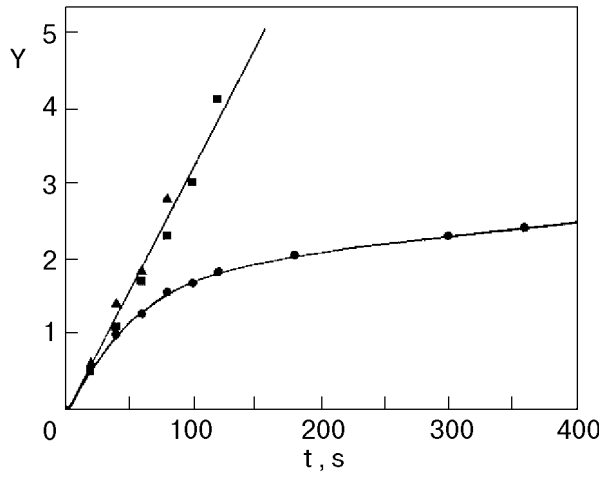


*Fig. 9.* Plots of $\ln (A^0_{O_3}/A^t_{O_3})$ (●), $\ln (A^0_{D_{ga}}/A^t_{D_{ga}})$ (▲), and $-\ln (1 - A^t_{H_2O_2}/A^{\infty}_{H_2O_2})$ (■), denoted as Y, versus the operating time of the laser at 266 nm (photon flux = $5{\cdot}10^{16}$ photons·$cm^{-2}$·$s^{-1}$) for a $H_2O/O_3$ mixture ($H_2O/O_3$ = 4) deposited and irradiated at 17 K.

$-\ln [(A^{\infty}_{H_2O_2} - A^t_{H_2O_2})/A^{\infty}_{H_2O_2}]$ versus irradiation times for a typical experiment (photon flux = $5{\cdot}10^{16}$ photons·$cm^{-2}$·$s^{-1}$) are shown in Fig. 9. The kinetics of $H_2O_2$ and of the $-O-H{:}O_3$ complex conforms to a first-order process with an apparent rate constant of $(3.5 \pm 0.5){\cdot}10^{-2}$ $s^{-1}$ (photon flux = $5{\cdot}10^{16}$ photons·$cm^{-2}$·$s^{-1}$) whereas the ozone kinetics does not conform to a first-order process. Two distinct phases are observed. The first phase shows the same linear dependence versus time as observed for $H_2O_2$ and $-O-H{:}O_3$ curves, whereas the second phase, at longer times, is characterized by a smaller plot with an apparent rate constant of $6{\cdot}10^{-4}$ $s^{-1}$. Such kinetic curves have also been found for photodissociation of solid ozone [9] and ozone trapped in argon matrices [28] and have not been accurately explained. In fact, as recently demonstrated by Kriachtchev et al. [29], during photolysis in the condensed phase the medium becomes more absorbing and leads to decrease of the laser intensity with depth. Thus the photolysis is more efficient near the surface as compared with deeper in the bulk, where it slows down with time. As a matter of fact, the kinetic rates at the same photon flux on a thicker water ice film were lowered.

### *5.2. Annealed mixture*

A $H_2O/O_3$ mixture (initial ratio 4) was deposited at 40 K and slowly annealed at 130 K till the disappearance of the associated OH band ($D_{ga}$); this process was accompanied by the formation of partially cubic ice. Then the sample was cooled at 17 K and irradiation was carried out at 266 nm with the same photon flux used previously. Growth of the 2858 $cm^{-1}$ band was observed, indicating that $H_2O_2$ in this experiment is produced by reaction of the $O(^1D)$ atom with the nearest $H_2O$ molecules. Two unexpected observations were made. First, the $\nu_2$ band of hydrogen peroxide at 1425 $cm^{-1}$ did not appear. Secondly, the ratio of integrated intensities between the 2858 $cm^{-1}$ band, which appeared at the end of irradiation, and the ozone band at 1031.5 $cm^{-1}$, which disappeared totally after 10 min, was very different from that observed after irradiation of unannealed mixtures, as illustrated in Fig. 10. It was found to be 25, a value forty times larger than the ratio found previously. The following explanations can be suggested for these observations.

Absence of the $\nu_2$ band of hydrogen peroxide can be due to our configuration using infrared reflection with an angle of incidence of 5°. Indeed, with this near-normal incidence at the surface, due to the

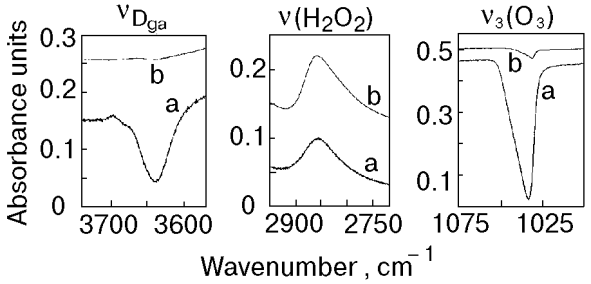


*Fig. 10.* Comparison of the key region of the difference vibrational spectra between spectra recorded before irradiation and after irradiation at 17 K of a $H_2O/O_3$ mixture deposited at 17 K (*a*) and of a $H_2O/O_3$ mixture annealed at 130 K and then cooled at 17 K (*b*).

metal surface selection rules, only the transverse optical mode, with a transition dipole moment parallel to the surface, can be excited. Thus in ordered ice the $H_2O_2$ molecule produced by the reaction of atomic oxygen with a water molecule could have an orientation preventing the observation of the 1425 $cm^{-1}$ band.

In the first set of experiments, (unannealed mixtures deposited at 17 K) the $\nu_3$ ozone band corresponds not only to complexed ozone but also to pure condensed ozone on the surface or in the pores. Only the hydrogen-bonded complex between ozone and water produces hydrogen peroxide, and hence the ratio between the intensities of the 2858 $cm^{-1}$ and the 1033 $cm^{-1}$ absorption lines can be weaker than that observed after irradiation of isolated ozone trapped in the ice lattice. This explanation is in agreement with the temperature effects described in Sec. 4.1.2, which showed that a very small amount of ozone resides in the lattice. The great difference between initial ozone in the two experiments (Fig. 10) that produced the same amount of $H_2O_2$ by irradiation indicates that deposition of a $H_2O/O_3$ mixture at 17 K leads mainly to ozone multilayers in pores and voids. However, a difference in the IR absorption coefficients between ozone on the ice surface and ozone inside the water lattice cannot be ruled ont.

Kinetic studies of the appearance of $H_2O_2$ and of the disappearance of ozone were carried out. The same shape of the kinetic curves was observed for $H_2O_2$ and $O_3$ . The curves were similar to that previously observed for ozone (see Fig. 9) with a rate, at short times, of the same order of magnitude $(4.0 \pm 0.5)\cdot10^{-2}$ $s^{-1}$ for a photon flux of $5\cdot10^{16}$ photons$\cdot cm^{-2}\cdot s^{-1}$. Recall that the photokinetic rate constant $k(\lambda)$ depends on the photodissociation cross section $\sigma(\lambda)$ in $cm^2$/molecule (base e) of ozone at 266 nm, the quantum yield $\varphi(\lambda)$, and the photon flux $F(\lambda)$ in photons$\cdot cm^{-2}\cdot s^{-1}$:

$$k(\lambda) = \sigma(\lambda)\varphi(\lambda)F(\lambda) .$$

Thus at short times the photodissociation of ozone forming an O ($^1D$) atom appears with the same apparent quantum yield for ozone in the $-O-H : O_3$ complex, pure condensed ozone (as verified in a subsequent experiment where amorphous pure ozone was irradiated under the same experimental conditions), and ozone in the lattice. Unfortunately, in the absence of knowledge of the photoabsorption cross sections of ozone at 266 nm in water ice and in the condensed state, it is not possible to calculate it. Indeed, as was shown by Vaida et al. in the visible [30] and also qualitatively in this laboratory [31–33], the absolute photoabsorption cross sections of species in condensed matter can be strongly modified with respect to their values in the gas phase.

Some information on the photolytic process can be obtained from the value of the rate constant found in our experiments. The kinetic rate of about $3.5\cdot10^{-2}$ $s^{-1}$ at short times is comparable to the kinetic rate found for the photodissociation of ozone in nitrogen [31] at a comparable photon flux and hence very different from the kinetic rate found for the photodissociation of ozone in argon matrices ($9\cdot10^{-4}$ $s^{-1}$) [28]. In the argon matrix but not in nitrogen matrix, the major pathway of ozone photodissociation is the reformation of ozone in the cage from photofragments O and $O_2$ , and the weak decrease of ozone is due to the exit of oxygen atom from the cage. A different situation is observed in water ice. As in the nitrogen matrix, photodissociation of ozone in ice is followed by the reaction of excited atomic oxygen with host molecules. Thus the possibility that the photogenerated O($^1D$) atoms may be quickly quenched to O($^3P$) atoms by collisions with the water molecule and then recombine with molecular oxygen appears as a slight probability. Unfortunately, the ratio between the IR absorption coefficients of the 2858 $cm^{-1}$ absorption ($H_2O_2$) and the 1033 $cm^{-1}$ band ($O_3$) is unknown, and the efficiency (probably very high) of the reaction between the mobile O($^1D$) atom and a nearest water molecule of the ice lattice cannot be accurately estimated.

Although much work remains in extending and quantifying our irradiation experiments, the results obtained in this pioneering work may be of interest in planetology. In particular, the formation of hydrogen peroxide by both the photodissociation of an $-O-H:O_3$ complex and the reaction of an O($^1D$)

atom with host water molecules has been demonstrated. Hydrogen peroxide has not been identified on Ganymede and other icy satellites of the solar system because it has no spectral absorption in the visible. The presence of $H_2O_2$ has to be taken into account for evaluating quantitatively the amount of $O_3$ produced from $O_2$ in ice. Furthermore, dissociation of $H_2O_2$ into OH radicals can lead to subsequent reactions. Future experiments are planned in this laboratory. In particular, the determination of the UV photoabsorption cross sections of ozone in ice and its formation through the photodissociation of oxygen trapped in amorphous water ice and amorphous ice containing sulphur dioxide will be studied.

## Acknowledgment

This work was supported in part by Programme National de Chimie Atmosphérique and Programme National de Planétologie.

1. L. Schriver-Mazzuoli, A. Shriver, C. Lugez, A. Perrin, C. Camy-Peyret, and J. M. Flaud, *J. Mol. Spectrosc.* **176**, 85 (1996).
2. J. R. Spencer, *J. Geophys. Res.* **100**, 19049 (1995).
3. W. M. Calvin, R. E. Johnson, and J. R Spencer, *Geophys. Res. Lett.* **23**, 673 (1996).
4. K. S. Noll, R. E. Johnson, A. L Lane, D. L. Domingue, and H. A. Weaver, *Science* **273**, 341 (1996).
5. R. E Johnson and W. A. Jesser, *Astrophys. J.* **480**, L79 (1997).
6. K. S. Noll, T. L. Roush, D. P. Cruikshank, R. E. Johnson, and Y. J. Pendleton, *Nature* **388**, 45 (1997).
7. J. Gittus, *Irradiation Effects in Crystalline Solids*, Applied Science, London, (1978).
8. J. W. Chamberlain and D. A. Hunten, *Theory of Planetary Atmospheres*, Academic, New York (1987).
9 A. J. Sedlacek and C. A. Wight, *J. Phys. Chem.* **93**, 509 (1989).
10. P. Jenniskens and D. F. Blake, *Astrophys. J.* **473**, 1113 (1996).
11. G. A. Baratta, G. Leto, F. Spinella, G. Strazzulla, and G. Foti, *Astron. Astrophys.* **252**, 421 (1991).
12. R. L. Hudson and M. H. More, *J. Phys. Chem.* **96**, 6500 (1992).
13. A. Kouchi and T. Kuroda, *Nature* **344**, 134 (1990).
14. E. Mayer and R. Pletzer, *Nature* **319**, 298 (1986).
15. J. A. Ghormley, *J. Chem. Phys.* **48**, 503 (1968).
16. B. Schmitt, J. Ocampo, and J. Klinger, *J. Phys.* (*Paris*) **48**, C1, 519 (1987).
17. B. S. Berland, D. E. Brown, M. A. Tolbert, and S. M. George, *International Symposium Physics and Chemistry of Ices, Lebanon*, New Hampshire, USA, August 26–30 (1996).
18. L. Schriver-Mazzuoli and A. Schriver, *J. Mol. Struct.* submitted.
19. H. Chaabouni, L. Schriver-Mazzuoli, and A. Schriver, *J. Chem. Phys.* submitted.
20. D. Laufer, E. Kochavi, and A. Bar-Nun, *Phys. Rev.* **B36**, 9219 (1987).
21. A. Bar-Nun, G. Herman, D. Laufer, and M. L. Rappaport, *Icarus* **63**, 317 (1985).
22. A. Kouchi, *J. Crystal Growth* **99**, 1220 (1990).
23. A. Givan, A. Loewenschuss, and C. J. Nielsen, *Vibrational Spectrosc.* **12**, 1 (1996).
24. S. A. Sandford and L. J. Allamendola, *Icarus* **76**, 201 (1988).
25. H. A. Michelsen, R. J. Salawitgh, P. O. Wennberg, and J. G. Anderson, *Geophys. Res. Lett.* **21**, 2227 (1994).
26. J. A. Lannon, F. D. Verderame, and R. W. Anderson, *Jr., J. Chem. Phys.* **54**, 2112 (1971).
27. L. Schriver-Mazzuoli, C. Barreau, and A. Schriver, *Chem. Phys.* **140**, 429 (1990).
28. M. Bahou, L. Schriver-Mazzuoli, and A. Schriver, *J. Chem. Phys.* **110**, 8636 (1999).
29. L. Kriachtchev, M. Petterson, and M. Rasanen, *Chem. Phys. Lett.* **299**, 727 (1998).
30. V. Vaida, D. J. Donaldson, S. J. Strickler, S. L. Stephens, and J. W. Birks, *J. Phys. Chem.* **93**, 506 (1989).
31. M. Bahou, L. Schriver-Mazzuoli, C. Camy- Peyret, and A. Schriver, *J. Chem. Phys.***108**, 6884 (1998).
32. A. Hallou, L. Schriver-Mazzuoli, A. Schriver, and P. Chaquin, *Chem. Phys.* **237**, 251 (1998).
33. M. Bahou, L. Schriver-Mazzuoli, A. Schriver, and P. Chaquin, *Chem. Phys.* **216**, 105 (1997).